Journal of Power Sources 196 (2011) 4613–4618

Contents lists available at ScienceDirect

Journal of Power Sources

journal homepage: www.elsevier.com/locate/jpowsour

Preparation of $LiFePO_4$/C composites by co-precipitation in molten stearic acid

Dragana Jugović[a,*], Miodrag Mitrić[b], Maja Kuzmanović[a], Nikola Cvjetićanin[c], Srečo Škapin[d], Božidar Cekić[b], Valentin Ivanovski[b], Dragan Uskoković[a]

[a] Institute of Technical Sciences of the Serbian Academy of Sciences and Arts, Knez Mihailova 35/IV, 11 000 Belgrade, Serbia
[b] The Vinča Institute of Nuclear Sciences, P.O. Box 522, 11 001 Belgrade, Serbia
[c] Faculty of Physical Chemistry, University of Belgrade, Studentski trg 12-16, P.O. Box 137, Belgrade, Serbia
[d] Jožef Štefan Institute, Jamova 39, SI-1000 Ljubljana, Slovenia

ARTICLE INFO

Article history:
Received 2 December 2010
Received in revised form 11 January 2011
Accepted 16 January 2011
Available online 26 January 2011

Keywords:
Lithium iron phosphate ($LiFePO_4$)
Rietveld analysis
Mössbauer spectroscopy
Cathode

ABSTRACT

The olivine type $LiFePO_4$ is synthesized via a simple and inexpensive route by aqueous co-precipitation of an Fe(II) precursor material in molten stearic acid and subsequent heat treatment at different temperatures. Stearic acid serves as both chelating agent and carbonaceous material. The obtained composites with carbon are characterized by X-ray powder diffraction, field emission scanning electron microscopy, and Mössbauer spectroscopy. Electrochemical characteristics of the composites are evaluated by using galvanostatic charge/discharge tests. The powder obtained at 700 °C delivers discharge capacity of 160 mAh g^{-1}, quite near the theoretical value.

1. Introduction

Recent review on challenges facing the development of rechargeable Li batteries for electric vehicles emphasized their cost, safety, cell energy density, rate of charge/discharge, and service life [1]. The olivine type $LiFePO_4$ is among the most attractive materials for the cathode of lithium-ion battery that meets the above criteria. The benefits of using $LiFePO_4$ are: excellent cycle life, high structural stability, low cost and environmental friendliness. Lithium iron phosphate can utilize one lithium ion per formula unit which leads to the theoretical capacity of 170 mAh g^{-1}. The first attempts to de-insert Li from this material were limited to about 0.6 e^- owing to transport limitations of electrons and ions [2]. There are several possible means to overcome this main obstacle in reaching theoretical capacity, that is its low electronic and/or ionic conductivity: by selective doping with supervalent cations [3–5], coating particles with electronically conductive agent such as carbon [6–9], Ag [10], RuO_2 [11], etc., and by decreasing particle size [12–14].

The olivine structure that typifies $LiFePO_4$ has a slightly distorted hexagonally close-packed oxygen array. The cation arrangement in $LiFePO_4$ differs significantly from that in the layered and spinel structures. The divalent Fe^{2+} ions occupy corner-shared octahedra (denoted as M2 sites). The phosphorus ions are located in tetrahedral sites, and the lithium ions reside in chains of edge-shared octahedra (M1 sites) [2,15]. Lithium motion within the olivine crystal structure occurs through one-dimensional (1D) channels along the *b* axis [16]. These one-dimensional paths are particularly susceptible to blockage by defects and impurities [16,17].

There are many synthesis routes in preparing $LiFePO_4$ [18]. Its commercial use has already started and there are several companies that base their business on lithium phosphate technology. Still, there is a need for a manufacturing process that produces electrochemically active $LiFePO_4$ at a low cost. Furthermore, simplicity of the synthesis process is vital for commercializing Li-ion batteries. Therefore, the interest in developing new approaches to the synthesis of $LiFePO_4$ did not fade.

Here is presented very simple and inexpensive route for obtaining $LiFePO_4$/C composites by aqueous co-precipitation of an Fe(II) precursor material in molten stearic acid and subsequent heat treatment in argon atmosphere at different temperatures. Stearic acid serves as both surfactant and dispersant, it is cheap and environmental friendly, and provides a stable environment for moisture sensitive precursors because of its hydrophobic nature. During pyrolytic degradation stearic acid decomposes in several steps that include decarboxylation, cracking and finally decomposition to carbon while creating reductive atmosphere that can prevent Fe^{2+} oxidation [19]. The *in situ* formed carbon would effectively restrict the growth of the particles, and by coating the particles would increase powder conductivity.

* Corresponding author. Tel.: +381 641177549; fax: +381 112185263.
E-mail addresses: dragana.jugovic@itn.sanu.ac.rs, djugovic@vinca.rs (D. Jugović).

0378-7753/$ – see front matter © 2011 Elsevier B.V. All rights reserved.
doi:10.1016/j.jpowsour.2011.01.072

2. Experimental

$LiFePO_4$/C composites were synthesized by an aqueous co-precipitation of an Fe(II) precursor material in the presence of stearic acid. Stearic acid was melted and then appropriate amount of aqueous solution of $(NH_4)_2HPO_4$ was added to it. Equimolar amounts of $FeSO_4 \cdot 7H_2O$ (Fluka) and $LiNO_3$ were dissolved in sufficient amount of water. This solution was added drop by drop into the heated melt under vigorous stirring when the precipitation occurred. The final molar ratio of Li:Fe:P:stearic acid was 1:1:1:1. After the evaporation of water, the melt was cooled to room temperature, thoroughly mixed and reground, and calcined at temperatures of 600, 700, and 800 °C in argon atmosphere. Thus obtained powders were washed with distilled water and dried under vacuum.

X-ray diffraction data were collected on a Philips PW 1050 diffractometer with Cu-K$\alpha_{1,2}$ radiation (Ni filter) at the room temperature. Measurements were done in 2θ range of 10–120° with scanning step width of 0.02° and 14 s times per step. Crystal structure refinement was based on the Rietveld full profile method [20] using the Koalariet computing program [21].

The Mössbauer absorption spectrum was obtained in a standard transmission geometry with constant acceleration using a source of ^{57}Co in Rh (1.85 GBq) at room temperature. $LiFePO_4$ powder was prepared as Mössbauer absorber with a diameter of 15 mm sandwiched by aluminium foils. The data were stored in 1024 multichannel analyzer. Laser spectrum and calibration spectra were recorded and fitted in order to recalculate channels in mm s^{-1}. The spectrum of sample synthesized at 800 °C has been examined by fitting data with WinNormos-Site program using a least squares method, while the other two samples were examined with WinNormos-Dist based on histogram method. Isomer shifts are shown with respect to α-Fe.

Thermal analysis of the sample was performed on SDT 2960 simultaneous DSC–TGA TA Instruments in order to determine carbon content [22].

The morphologies of the synthesized powders were analyzed by field emission scanning electron microscopy (FE-SEM, Supra 35 VP, Carl Zeiss).

Electrochemical measurements were carried out in a closed, argon filled two-electrode cell at room temperature, with metallic lithium as a counter electrode. 1 M solution of $LiClO_4$ (p.a., Chemmetall GmbH) in PC (p.a., Honeywell) was used as electrolyte. Working electrodes were made from synthesized material, carbon black and polyvinylidene fluoride (PVdF, Aldrich) mixed in 75:20:5 weight percent ratio and deposited on platinum foils from slurry prepared in N-methyl-2-pyrrolidone. Galvanostatic charge/discharge tests were performed between 4.1 and 2.5 V at C/10 current rates.

3. Results and discussion

Fig. 1 shows particle morphologies of the samples revealed by field emission scanning electron microscopy (FESEM). At the lowest temperature of 600 °C the particles are highly agglomerated, consisted of closely packed cauliflower-like nodular structures giving rise to irregularly shaped pores of variable width. The primary grains are less than 50 nm in size. Particle bonding and neck formation, denoting interparticle sintering, can be observed as well. By increasing the temperature to 700 °C the morphology does not change a lot. Apparently, the *in situ* formed carbon effectively restricted the growth of the particles. Going to the highest temperature of 800 °C there is remarkable difference in morphology, actually two different particle morphologies can be observed. Besides previously seen nodular morphology there are a great

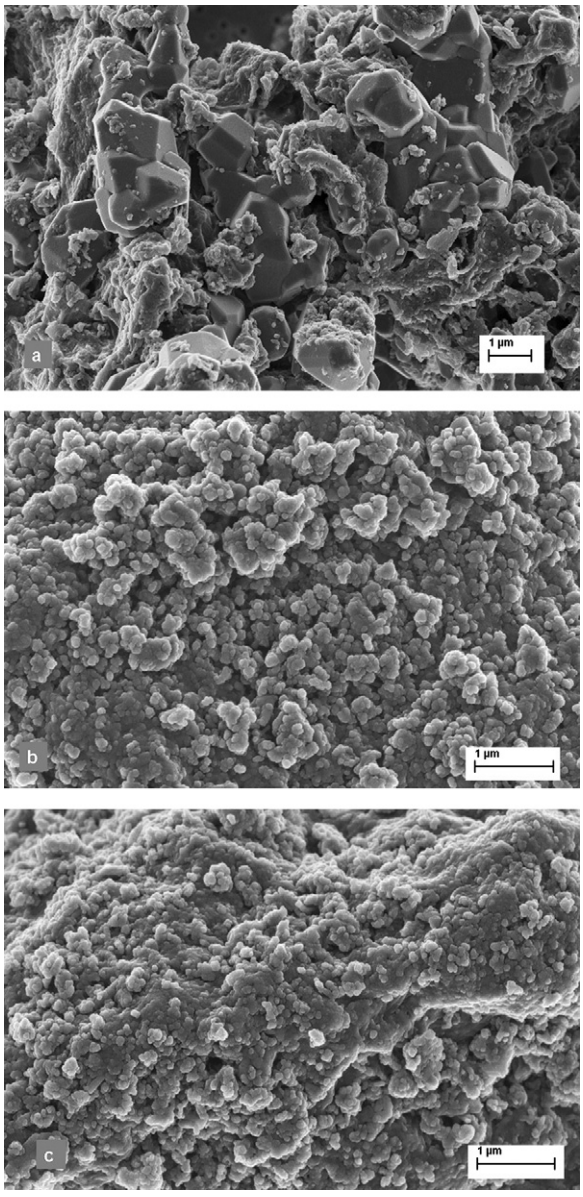

Fig. 1. FESEM micrographs of the powders obtained at (a) 800 °C, (b) 700 °C, and (c) 600 °C.

number of agglomerated micron-sized polyhedra that are most probably grown on the account of small grains. Such polyhedral crystal shape is comparable to the theoretically calculated growth morphology of $LiFePO_4$ [23]. Apparently, the temperature of 800 °C was sufficient for enabling further crystallization and growth of the primary particles.

X-ray powder diffraction patterns (Fig. 2) were used for phase identification and structural analysis. In all three samples olivine type $LiFePO_4$ was obtained as a major phase with heterosite $FePO_4$ as a minor phase. A two-phase refinement was performed on XRD data to quantify the amounts of different phases present. The amount of the second phase is increasing with increasing calcination temperature, starting from 9 wt% (Table 1) at the lowest temperature and reaching almost 15 wt% (Table 1) at the highest temperature. This finding is quite surprising since, according to the literature, heterosite $FePO_4$ is obtainable only by chemical or electrochemical delithiation of olivine $LiFePO_4$ phase [24]. To our best knowledge, it has never been synthesized or even found as an impurity phase before. Furthermore, on heating, heterosite

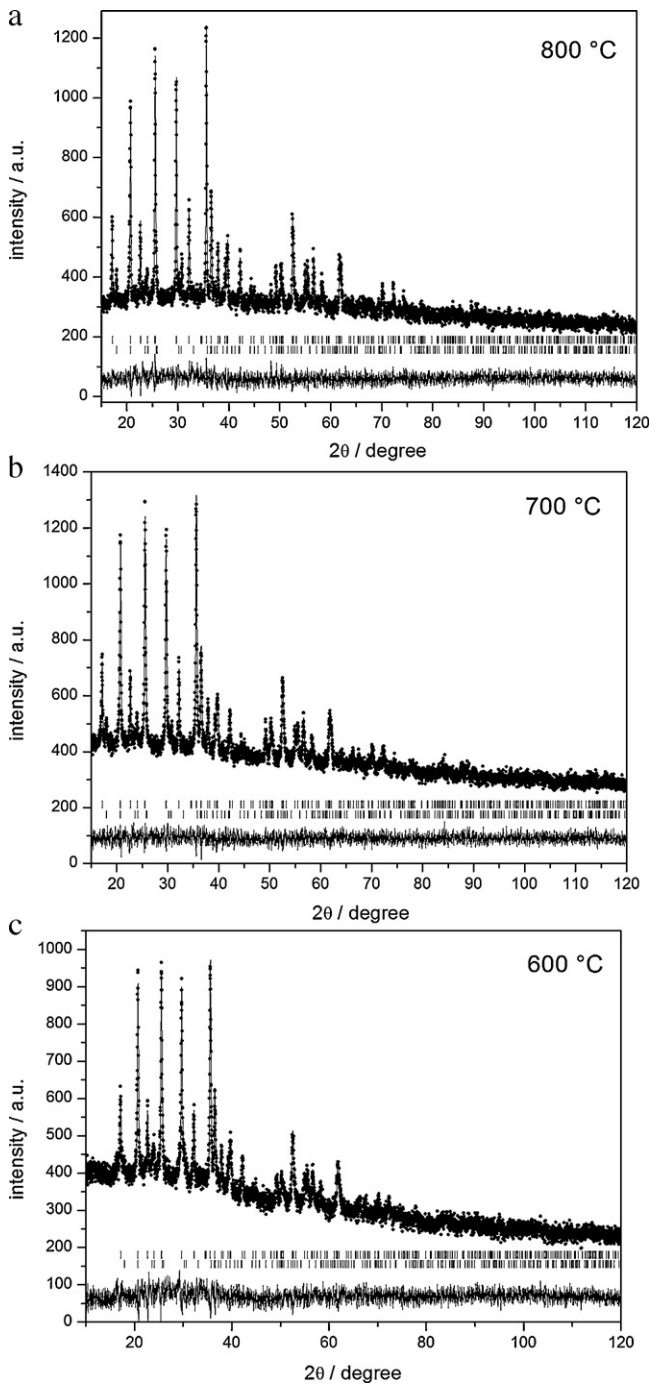

Fig. 2. The observed (●), calculated (–), and the difference between the observed and calculated (bottom) X-ray diffraction data taken at room temperature from the powders thermally treated at (a) 800 °C, (b) 700 °C, and (c) 600 °C under argon atmosphere. Vertical markers bellow the diffraction patterns indicate positions of possible Bragg reflections for olivine type $LiFePO_4$ (upper) and heterosite $FePO_4$ (lower).

$FePO_4$ irreversibly converts to the electrochemically inactive trigonal verlinite phase $FePO_4$ [22]. At temperatures higher than 200 °C $LiFePO_4$ and $FePO_4$ make solid solution forming lithium deficient olivine phase Li_xFePO_4 ($x < 1$) that on cooling back to room temperature separates into mixtures of $LiFePO_4 + FePO_4$ [25,26]. Recently, solid–solution phases in Li_xFePO_4 close to the stoichiometric end members $LiFePO_4$ and $FePO_4$ were successfully isolated at room temperature using both chemical and electrochemical routes [27,28]. On further heating at temperatures greater than 500 °C, solid solution Li_xFePO_4 starts to decompose into mixtures of non-olivine compounds [25]. These imply that during our synthesis lithium deficient olivine type Li_xFePO_4 was formed, which upon cooling separates into mixtures of $LiFePO_4 + FePO_4$. Apparently, atmosphere conditions where such that enabled the preservation of the olivine structure, even though high temperatures (higher than 500 °C) were applied. Li_2O was detected by XRD as the third phase in sample obtained at 800 °C before it was washed with water. Obviously, departure of lithium from the structure and reaction with O_2 is temperature dependent, but its cause is still not apparent. Li_2O decomposes after washing the powders with water, and hence does not exist in the powders under investigation. There is no evidence for the formation of crystalline carbon, so internal carbon could be treated as a contribution to the background. The amount of an *in situ* formed carbon was determined by heating the powder in air considering that only Fe^{2+} ions oxidize and contribute to the weight gain. Taken in account the amount of Fe^{2+} ions obtained by Mössbauer spectroscopy the estimated amounts of carbon were ranging from 5 to 4 wt% with increasing temperature. In addition, energy dispersive spectroscopy (EDS) of the samples showed only peaks corresponding to Fe, P, C, and O. Li is too light for the detection with EDS.

Crystal structure refinements were based on the Rietveld full profile method [20] using the Koalariet computing program based on a Fundamental Parameters convolution approach to generate line profiles [21]. This program is appropriate for processing the data obtained from the samples with dominant microstructure parameters (small crystallite size and large microstrains). The observed and calculated X-ray diffraction profiles of the samples are given in Fig. 2, while the main results of the final Rietveld refinements are presented in Tables 1 and 2. The structure of both $LiFePO_4$ and $FePO_4$ powders have been refined in the space group Pnma ($D_{2h}{}^{16}$) in olivine type with following crystallographic positions: Li^+ ions in special crystallographic position 4*a* [0,0,0] with local symmetry $\bar{1}$; Fe^{2+} and P^{5+} ions occupy two different crystallographic 4*c* positions [*x*,0.25,*z*] with local symmetry m; O^{2-} ions occupy three different crystallographic positions: additional two 4*c* positions and one general 8*d* position [*x*,*y*,*z*] with local symmetry 1. The Rietveld refinement results indicate that lattice parameters and primitive cell volumes of each phase are similar for all three samples and consistent with the literature data [15]. Primitive cell volume of olivine $LiFePO_4$ phase is near 291.7 Å^3, regardless of the synthesis temperature, very much the same as the volume of hydrothermally obtained single crystal [29]. The main differences are in microstructural parameters: mean crystallite size, microstrain and strain. The obtained values for microstrain and strain are refined to zero within an error, and therefore cannot be quantified by number, still the trend that follows with increasing temperature is a decrease of microstrain, and an increase of strain. The value for mean crystallite size increases from 56 nm to 140 nm with increasing temperature. Material synthesized at the highest temperature presents the largest coherence domain length with no microstrain, and with noticeable strain. The Rietveld refinement also showed additional electron density on the lithium sites indicating so-called "anti-site" defect in which a Li ion (on the M1 site) and an Fe ion (on the M2 site) are interchanged. This anti-site disorder (ca. 1–2 mol%) is believed to be intrinsic property of olivine $LiFePO_4$ [17]. Powder obtained at 600 °C has the highest value of this disorder suggesting 3 at.% occupation of Li sites by Fe. It is not possible from powder Rietveld studies to differentiate between an iron-rich model, $Li_{1-2y}Fe_yFePO_4$, and a lithium–iron mixing model, $Li_{1-y}Fe_y[Li_yFe_{1-y}]PO_4$, with only Fe^{2+} ions taking into consideration, or to exclude the existence of both cation vacancies and anti-site disorder $(\square_x Li_{1-x-y}Fe_y)(\square_z Fe_{1-z})PO_4$ with lithium deficiency and the presence of significant amounts of Fe at the oxidation state +3. By comparing mean crystallite size with the mean

Table 1
The final results of the two-phase Rietveld structural refinement of the samples obtained at 800 °C, 700 °C, and 600 °C.

Thermal treatment temperature (°C)	600		700		800	
Lattice parameters (Å)	$LiFePO_4$	$FePO_4$	$LiFePO_4$	$FePO_4$	$LiFePO_4$	$FePO_4$
	a = 10.3241(3)	a = 9.8635(7)	a = 10.3279(3)	a = 9.8439(4)	a = 10.3345(6)	a = 9.8304(2)
	b = 6.0096(2)	b = 5.8339(4)	b = 6.0096(2)	b = 5.8089(2)	b = 6.0101(3)	b = 5.7995(1)
	c = 4.7023(2)	c = 4.7645(4)	c = 4.6994(1)	c = 4.7809(2)	c = 4.6957(3)	c = 4.7828(1)
Primitive cell volume (Å^3)	V = 291.75(2)	V = 274.16(3)	V = 291.68(9)	V = 273.38(9)	V = 291.66(6)	V = 272.67(9)
Weight (%)	90.6(1)	9.4(1)	88.7(1)	11.3(1)	85.1(1)	14.9(1)
Mean crystallite size (nm)	57(3)		75(4)		140(10)	
Li site occ. by Fe	0.027(7)		0.019(5)		0.020(5)	
R factor (%)	Rwp = 4.43		Rwp = 3.76		Rwp = 4.49	

particle size estimated from FESEM images it can be concluded that at the lowest temperature of 600 °C part of the particles could be considered as single nanocrystals, whereas at higher temperatures particles are polycrystalline composed of a number of crystallites. The refinement results imply that thermal treatment at 700 °C is optimal for obtaining powder consisted of small particles with good crystallinity and iron ordering (Table 1), all of them being necessary for delivering good electrochemical properties.

Asymmetric Mössbauer absorption spectra revealed the presence of Fe^{2+} and Fe^{3+} ions. As shown in Fig. 3, three doublets were required to adjust the calculated spectrum to the experimental one. There are no lines that could be attributed to sextet originated in Fe_2O_3 impurity. The characteristic parameters deduced from these refinements (Table 3) imply the presence of Fe^{2+} and Fe^{3+} in octahedral coordination, assigned to olivine $LiFePO_4$ and heterosite $FePO_4$, respectively [30], but also the presence of Fe^{3+} ions in tetrahedral coordination. According to the Mössbauer study, molar ratio of octahedrally coordinated Fe^{2+}/Fe^{3+} is smaller than the Fe^{2+}/Fe^{3+} ratio of crystallized phases calculated from the Rietveld two-phase refinement, meaning that octahedrally coordinated Fe^{3+} ions are present not only in heterosite, but also in olivine phase within composite powder. Ferric iron can arise in two ways: either by ion replacement $3Fe^{2+} \rightarrow 2Fe^{3+}$, leaving a vacancy in the M(2) site, or by the replacement process $Li^+Fe^{2+} \rightarrow Fe^{3+}$, leaving a vacancy in the M(1) site [15]. This leads to the conclusion that olivine phase in the sample is lithium deficient Li_xFePO_4 where lithium ion was replaced by Fe^{3+} ion creating both cation vacancies and anti-site disorder, the latter revealed by Rietveld refinement. The determined full widths at half maximum (Γ) for the two differently coordinated Fe^{3+} ions were significantly different, with Γ around 0.3 mm s^{-1} for the octahedrally coordinated Fe^{3+} ions and around 0.6 mm s^{-1} for the tetrahedrally coordinated Fe^{3+} ions. This large broadening of the Fe^{3+} Mössbauer absorption line suggests the existence of a distribution of quadrupolar effects [31], so additionally quadrupole splitting distribution was included in the fitting procedure. The two unimodal distributions are obtained for the sample synthesized at 700 °C, while the bimodal distribution is present for the sample synthesized at 600 °C. The average values of isomer shifts for named three distributions are approximately the same and are attached to the presence of ferric ions. The first peak in the bimodal distribution is positioned at $\Delta \approx 0.20$ mm s^{-1}, and the second one at $\Delta \approx 0.90$ mm s^{-1}. The distribution is related to the structural distortion in the environment of the absorbing ion, which could be associated with amorphous or nanoparticulate nature of this Fe^{3+} phase, which is of low crystallinity, and therefore not detectable by X-ray diffraction. Note that our samples were synthesized in a short time that can promote formation of residual amorphous impurities. Trivalent Fe might be formed during thermal treatments by a small amount of oxygen that is always included in argon flow, so it is probably better to use a gas mixture of argon with few percentages of hydrogen during the thermal treatments.

Electrochemical performances of the samples used as a cathode of a Li-ion battery were examined by charge–discharge tests. For all samples a flat plateau at around 3.4 V is observed during both charge and discharge (Fig. 4), implying typical two-phased deintercalation/intercalation reaction. Resulted specific capacities

Table 2
Fixed and refined atomic coordinates and isotropic displacement parameters in $LiFePO_4$ and $FePO_4$ phases present in the samples.

Thermal treatment temperature 600 °C							
	$LiFePO_4$			$FePO_4$			
Fractional coordinates	x	y	z	x	y	z	B (Å^2)
Li (4a)	0	0	0	–	–	–	1.8(1)
Fe (4c)	0.2824(4)	0.25	0.9766(1)	0.2822(4)	0.25	0.9568(1)	1.8(1)
P (4c)	0.0925(9)	0.25	0.4107(2)	0.1090(8)	0.25	0.4251(2)	1.8(1)
O(1) (4c)	0.1081(2)	0.25	0.7289(3)	0.1821(7)	0.25	0.7226(3)	1.8(1)
O(2) (4c)	0.4518(3)	0.25	0.2107(3)	0.4821(7)	0.25	0.2156(3)	1.8(1)
O(3) (8d)	0.1639(1)	0.0432(2)	0.28214(2)	0.1260(8)	0.0652(1)	0.2694(1)	1.8(1)
Thermal treatment temperature 700 °C							
Li (4a)	0	0	0	–	–	–	1.2(1)
Fe (4c)	0.2820(3)	0.25	0.9749(4)	0.2774(2)	0.25	0.9505(2)	1.2(1)
P (4c)	0.0924(4)	0.25	0.4140(6)	0.1052(4)	0.25	0.4048(5)	1.2(1)
O(1) (4c)	0.1039(6)	0.25	0.7343(7)	0.1519(7)	0.25	0.7457(5)	1.2(1)
O(2) (4c)	0.4563(6)	0.25	0.2100(7)	0.4299(7)	0.25	0.1714(6)	1.2(1)
O(3) (8d)	0.1682(1)	0.0426(7)	0.2828(6)	0.1442(5)	0.0436(7)	0.2578(2)	1.2(1)
Thermal treatment temperature 800 °C							
Li (4a)	0	0	0	–	–	–	1.1(1)
Fe (4c)	0.2822(3)	0.25	0.9762(4)	0.2712(2)	0.25	0.9418(3)	1.1(1)
P (4c)	0.0942(7)	0.25	0.4153(5)	0.0926(3)	0.25	0.3858(5)	1.1(1)
O(1) (4c)	0.1009(9)	0.25	0.7412(7)	0.1350(6)	0.25	0.6836(6)	1.1(1)
O(2) (4c)	0.4602(9)	0.25	0.2158(7)	0.4241(6)	0.25	0.1615(6)	1.1(1)
O(3) (8d)	0.1670(9)	0.0406(9)	0.2808(6)	0.1479(4)	0.0053(5)	0.2698(5)	1.1(1)

Table 3
Mössbauer parameters obtained by fittings for the powders thermally treated at 800 °C, 700 °C, and 600 °C.

Thermal treatment temperature (°C)	Site	A (%)	δ (mm s^{-1})	Δ (mm s^{-1})	Γ (mm s^{-1})
800	Fe^{2+} (O_h)	60(1)	1.205(2)	2.958(5)	0.286(6)
	Fe^{3+} (O_h)	23(2)	0.494(9)	1.33(2)	0.36(3)
	Fe^{3+} (T_h)	17(2)	0.36(1)	0.63(3)	0.40(4)
700	Fe^{2+} (O_h)	70(1)	1.210(1)	2.959(3)	0.311(4)
	Fe^{3+} (O_h)	19(2)	0.48(1)	1.32(3)	0.44(3)
	Distributions:		$\langle\delta\rangle$	$\langle\Delta\rangle$	SD
	Fe^{3+}	4.5	0.40(7)	0.264	0.116
	Fe^{3+}	6.5	0.42(7)	0.759	0.126
600	Fe^{2+} (O_h)	66(1)	1.208(7)	2.94(1)	0.332(9)
	Fe^{3+} (O_h)	10(6)	0.42(7)	1.5(2)	0.4(1)
	Distributions:		$\langle\delta\rangle$	$\langle\Delta\rangle$	SD
	Fe^{3+}	23.3	0.37(4)	0.65	0.316

δ, Δ, Γ, and A are isomer shift, quadrupole splitting, the full width at half maximum, and absorption area intensity ratio, respectively.

were calculated based on the mass of the powders as a whole, reduced only by the amount of estimated carbon. It is interesting to note that delivered capacity on first charging process (108 mAh g^{-1}, 116 mAh g^{-1}, and 106 mAh g^{-1} for the powders obtained at 800, 700, 600 °C, respectively) is smaller than that obtained on discharging for all samples. On the other hand, the first charge capacity is proportional to the amount of Fe^{2+} ions present in powders calculated by Mössbauer spectroscopy. The derived value of the discharge specific capacity for the powders obtained at 600 °C and 700 °C is about 160 mAh g^{-1}, which is quite near the theoretical value, showing that heterosite $FePO_4$ phase also participated in electrochemical reactions. Besides, discharging curves for the powders obtained at 600 °C and 700 °C show discrepancy between line profiles indicating dissimilar mechanism of lithium ion insertion. Namely, at 600 °C at certain lithium content discharging curve changes its profile from flat plateau to sloping curve indicating shift in Li insertion mechanism from two-phase process to a single-phase process. There are several possibilities for such behavior documented in the literature: (i) The third Fe^{3+} phase found by Mössbauer spectroscopy, which showed the existence of a distribution of quadrupolar effects, could be an amorphous trigonal $FePO_4$ phase, which is electrochemically active showing sloping charge/discharge curves [32,33]. The trigonal form is composed of iron and phosphorus atoms tetrahedrally bonded to four oxygen atoms [22], (ii) the voltage slope is a surface effect, which suggests that the amorphous surface layer containing Fe^{3+}($S = 1/2$) allows a more homogeneous distribution of Li and Li vacancies upon delithiation than the crystal, where iron is in the Fe^{2+}($S = 2$) state [34] and (iii) recently, it has been shown that the two-phase nature of the $LiFePO_4/FePO_4$ system changes into a

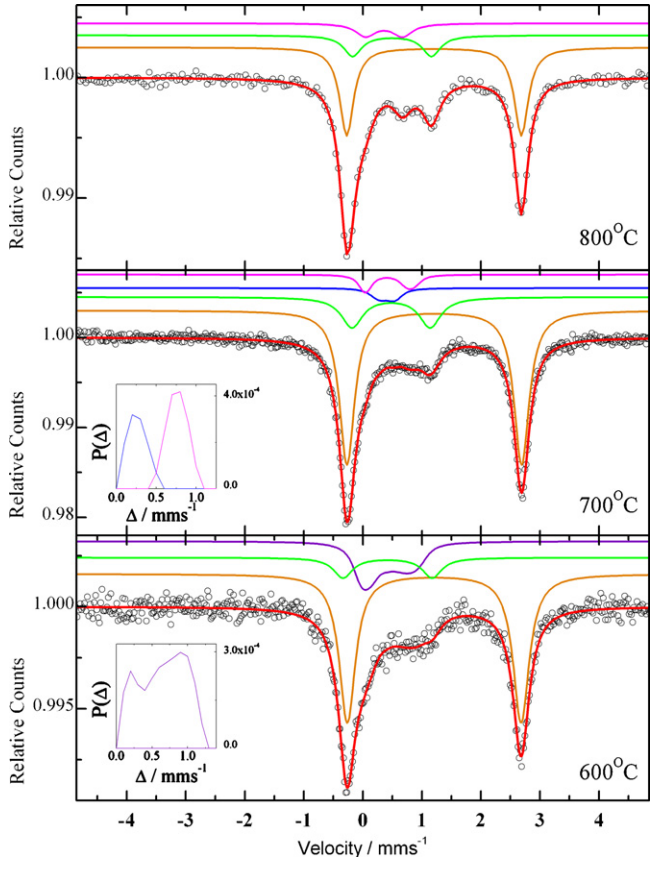

Fig. 3. Mössbauer spectra at room temperature for the powders obtained at 800 °C, 700 °C and 600 °C. Insets on the left side are the quadrupole splitting distributions.

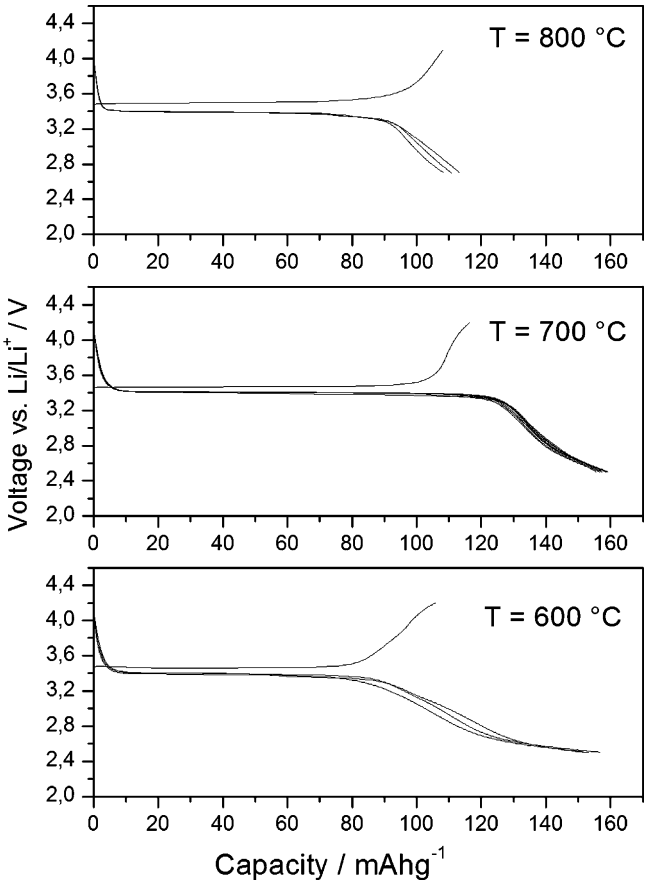

Fig. 4. Cycle performances of the synthesized powders at C/10 rate.

one-phase solid-solution Li_xFePO_4 system by downsizing the particles having large anti-site disorder [12]. As previously showed, the particles obtained at 600 °C were the smallest in size, having the largest anti-site disorder, and part of them can be treated as nanocrystals. Powder obtained at 800 °C delivered capacity of 110 mAh g^{-1}. Such capacity loss, compared to the other two powders, is a consequence of increased both crystallite and particle size that suppressed the whole utilization of the material due to their small surface area and an impediment of lithium ions to diffuse through the $LiFePO_4/FePO_4$ interface. In addition, the voltage hysteresis between the charge and discharge curve obtained during galvanostatic testing is the largest for the sample obtained at 800 °C, indicating the increase of impedance due to larger particle size since the electrode resistance depends solely on the mean particle size [13].

4. Conclusion

Simplicity of the synthesis process is vital for commercializing Li-ion batteries. Here we presented simple and inexpensive route for obtaining $LiFePO_4$/C composites by aqueous co-precipitation of an Fe(II) precursor material in the presence of stearic acid. Stearic acid serves as both surfactant and dispersant, which decomposes to carbon during pyrolytic degradation and creates reductive atmosphere that can prevent Fe^{2+} oxidation. The obtained powders were composites made of olivine type $LiFePO_4$ and carbon, and with heterosite $FePO_4$ as a minor phase evidenced for the first time in the literature as a byproduct of the synthesis. Nevertheless, the optimal powder delivered discharge capacity of 160 mAh g^{-1}, which is quite near the theoretical value, showing that heterosite $FePO_4$ phase also participated in electrochemical reactions. The discussed synthesis route does not suppose any specific or expensive equipment, and it can be easily scaled up for commercialization. This process also shows potential for further improvement by altering synthesis conditions to obtain fully electrochemically active $LiFePO_4$.

Acknowledgements

The Ministry of Science and Technological Development of the Republic of Serbia provided financial support under grant nos. III45004, III45015, and III45014.

References

[1] J.B. Goodenough, Y. Kim, Chem. Mater. 22 (2010) 587–603.
[2] A.K. Padhi, K.S. Nanjundswamy, J.B. Goodenough, J. Electrochem. Soc. 144 (1997) 1188–1194.
[3] S.-Y. Chung, J.T. Bloking, Y.-M. Chiang, Nat. Mater. 1 (2002) 123–128.
[4] G.X. Wang, S. Needham, J. Yao, J.Z. Wang, R.S. Liu, H.K. Liu, J. Power Sources 159 (2006) 282–286.
[5] G.X. Wang, S.L. Bewlay, K. Konstatinov, H.K. Liu, S.X. Dou, J.-H. Ahn, Electrochim. Acta 50 (2004) 443–447.
[6] M. Gaberšček, R. Dominko, M. Bele, M. Remškar, D. Hanžel, J. Jamnik, Solid State Ionics 176 (2005) 1801–1805.
[7] M.M. Doeff, J.D. Wilcox, R. Kostecki, G. Lau, J. Power Sources 163 (2006) 180–184.
[8] K. Kim, J. Hwa Jeong, I.-J. Kim, H.-S. Kim, J. Power Sources 167 (2007) 524–528.
[9] J.-K. Kim, J.-W. Choi, G.S. Chauhan, J.-H. Ahn, G.-C. Hwang, J.-B. Choi, H.-J. Ahn, Elactrochim. Acta 53 (2008) 8258–8264.
[10] K.S. Park, J.T. Son, H.T. Chung, S.J. Kim, K.T. Kang, H.G. Kim, Solid State Commun. 129 (2004) 311–314.
[11] Y.-S. Hu, Y.-G. Guo, R. Dominko, M. Gaberšček, J. Jamnik, J. Maier, Adv. Mater. 19 (2007) 1963–1966.
[12] P. Gibot, M. Casas-Cabanas, L. Laffont, S. Levasseur, P. Carlach, S. Hamelet, J.-M. Tarascon, C. Masquelier, Nat. Mater. 7 (2008) 741–747.
[13] M. Gaberšček, R. Dominko, J. Jamnik, Elactrochem. Commun. 9 (2007) 2778–2783.
[14] K. Saravanan, M.V. Reddy, P. Balaya, H. Gong, B.V.R. Chowdari, J.J. Vittal, J. Mater. Chem. 19 (2009) 605–610.
[15] A.S. Andersson, B. Kalska, L. Häggström, J.O. Thomas, Solid State Ionics 130 (2000) 41–52.
[16] D. Morgan, A. Van der Ven, G. Ceder, Electrochem. Solid-State Lett. 7 (2004) A30–A32.
[17] M.S. Islam, D.J. Driscoll, C.A.J. Fisher, P.R. Slater, Chem. Mater. 17 (2005) 5085–5092.
[18] Dragana Jugović, Dragan Uskoković, J. Power Sources 190 (2009) 538–544.
[19] K.D. Maher, K.M. Kirkwood, M.R. Gray, D.C. Bressler, Ind. Eng. Chem. Res. 47 (2008) 5328–5336.
[20] H.M. Rietveld, J. Appl. Cryst. 2 (1969) 65–71.
[21] R.W. Cheary, A. Coelho, J. Appl. Cryst. 25 (1992) 109–121.
[22] Sh. Yang, Y. Song, P.Y. Zavalij, M.S. Whittingham, Electrochem. Commun. 4 (2002) 239–244.
[23] C.A.J. Fisher, M.S. Islam, J. Mater. Chem. 18 (2008) 1209–1215.
[24] G. Rousse, J. Rodriguez-Carvajal, S. Patoux, C. Masquelier, Chem. Mater. 15 (2003) 4082–4090.
[25] Ch. Delacourt, Ph. Poizot, J.-M. Tarascon, Ch. Masquelier, Nat. Mater. 4 (2005) 254–260.
[26] Ch. Delacourt, J. Rodriguez-Carvajal, B. Schmitt, J.-M. Tarascon, Ch. Masquelier, Solid State Sci. 7 (2005) 1506–1516.
[27] A. Yamada, H. Koizumi, N. Sonoyama, R. Kanno, Electrochem. Solid-State Lett. 8 (2005) A409–A413.
[28] G. Kobayashi, Sh. Nishimura, M.-S. Park, R. Kanno, M. Yashima, T. Ida, A. Yamada, Adv. Funct. Mater. 19 (2009) 395–403.
[29] J. Chen, M.J. Vacchio, Sh. Wang, N. Chernova, P.Y. Zavalij, M.S. Whittingham, Solid State Ionics 178 (2008) 1676–1693.
[30] Z. Li, I. Shinno, Miner. J. 19 (1997) 99–107.
[31] M. Maccario, L. Croguennec, A. Wattiaux, E. Suard, F. Le Cras, C. Delmas, Solid State Ionics 179 (2008) 2020–2026.
[32] S. Okada, T. Yamamoto, Y. Okazaki, J. Yamaki, M. Tokunaga, T. Nishida, J. Power Sources 146 (2005) 570–574.
[33] Y. Song, Sh. Yang, P.Y. Zavalij, M.S. Whittingham, Mater. Res. Bull. 37 (2002) 1249–1257.
[34] K. Zaghib, A. Mauger, F. Gendron, C.M. Julien, Chem. Mater. 20 (2008) 462–469.